Applied Surface Science 525 (2020) 146594

Contents lists available at ScienceDirect

Applied Surface Science

journal homepage: www.elsevier.com/locate/apsusc

Electrochemically deposited poly(selenophene)-fullerene photoactive layer: Tuning of the spectroscopic properties towards visible light-driven generation of singlet oxygen

Aleksandra Nyga[a], Radoslaw Motyka[a], Gianlorenzo Bussetti[b], Alberto Calloni[b], Madan Sangarashettyhalli Jagadeesh[b], Sylwia Fijak[a], Sandra Pluczyk-Malek[a], Przemyslaw Data[a], Agata Blacha-Grzechnik[a,*]

[a] Faculty of Chemistry, Silesian University of Technology, Strzody 9, 44-100 Gliwice, Poland
[b] Department of Physics, Politecnico di Milano, Piazza Leonardo Da Vinci, 32, 20133 Milan, Italy

ARTICLE INFO

Keywords:
Photoactive layers
Visible light-driven singlet oxygen generation
Fullerene dyads
Photosensitizers immobilization
Electrochemical polymerization

ABSTRACT

A selenophene-containing fullerene dyad (C_{60}Se) was electrochemically co-deposited with bis-selenophene (BisSe) to form a visible light absorbing poly(selenophene) layer with incorporated fullerene photosensitizers on platinum (Pt) or indium-tin oxide (ITO) substrates. The resulting photoactive films (P(C_{60}Se_BisSe)) were characterized by cyclic voltammetry, UV–Vis, IR, Raman and X-ray photoelectron spectroscopies. The efficiency of P(C_{60}Se_BisSe) towards singlet oxygen photogeneration was investigated by applying reactions with chemical traps, *i.e.* α-terpinene and 1,3–diphenylisobenzofuran (DPBF), monitored by UV–Vis spectroscopy. The composition of the electropolymerized layer was controlled by varying the monomers ratio in the feed solution and it had a strong influence on the spectroscopic and photosensitizing properties of the deposited film. It has been shown that the efficiency of the visible light-driven singlet oxygen generation can be increased by optimizing the ratio between C_{60} photosensitizers and organic units in the layer.

1. Introduction

Lately, carbon nanostructures, *i.e.* fullerenes, nanotubes and graphene, have attracted considerable attention in the photocatalysis, because of their high efficiency of singlet oxygen ($^1O_2$) production [1,2]. Since such photosensitizers absorb mainly in the ultraviolet region, their spectroscopic properties have to be optimized. This can be done using different strategies that are generally based on the covalent attachment of a chromophore or incorporation into organic matrix absorbing in the visible region [3-8]. The resulting visible light-harvesting structures can be effectively applied as a source of $^1O_2$ molecule. This active form of oxygen can be simply produced in the photosensitization process, in which a photosensitizer molecule is activated by light illumination and transfers energy to triplet state oxygen via collision (so called Type II mechanism) [9-11]. Next to carbon nanostructures, other organic or inorganic photosensitizers show high photosensitizing efficiency: dyes, porphyrins, inorganic transition metals complexes or semiconductors oxides [10,12].

Among Reactive Oxygen Species (ROS), singlet oxygen possess one of the highest oxidative properties and reacts rapidly with an unsaturated carbon–carbon bond or with neutral nucleophiles. Singlet oxygen is extremely attractive as an oxidizing agent in the light-activated synthesis of fine chemicals, *i.e.* production of ascaridole, juglone etc., or in the wastewater treatment [1,9,13]. The lifetime of $^1O_2$ strongly depends on the type of solvent [14] - it can vary from few μs in water and methanol, up to few hundreds μs in chlorinated or deuterated ones [15]. Still, this active form of oxygen is relatively short-lived, and thus, it has to be generated *in situ* in a reaction mixture. Though, typically higher efficiency is observed for the homogenous photosensitization, the heterogeneous approach has many advantages, like simplified operation, product separation or recycling of a photocatalyst. In some cases even higher stability of the latter can be observed [1,16,17]. Various approaches for the deposition of photoactive molecules have been reported, e.g. based on the covalent immobilization on a solid support or non-covalent incorporation into a polymeric matrix [1,18,19].

The investigation of new solid fullerene-based photosensitizers should take into account the type of precursor and the strategy of the

* Corresponding author at: 44-100 Gliwice, Strzody 9, Poland.
E-mail address: agata.blacha@polsl.pl (A. Blacha-Grzechnik).

https://doi.org/10.1016/j.apsusc.2020.146594
Received 13 January 2020; Received in revised form 3 May 2020; Accepted 3 May 2020
Available online 07 May 2020

layer deposition, that would allow controlling the properties of both – the fullerene photosensitizer and the visible light absorbing unit. In our previous work we have shown that the structure of terthiophene-fullerene dyad strongly influences the photosensitizing efficiency of the resulting photoactive layer [20]. Till now, the organic layers containing thiophene and selenophene units have been mainly investigated for the application in the organic electronics, especially in the fullerene or non-fullerene Organic Photovoltaic Devices (OPVs) [21-24]. Lately, it has been shown that fullerene – conjugate polymers blends are able to generate ROS, including singlet oxygen. This, however, is considered as a drawback in solar cells, since it may result in a device degradation [25-29].

Here, we continue our studies aiming to increase the visible light absorption of the photoactive layer by the introduction of selected organic-only units absorbing in the low energy region. Thus, a selenophene/thiophene-fullerene dyad (C_{60}Se), chosen as a photoactive precursor was co-deposited with bis-selenophene (BisSe) in the electrochemical polymerization process. The main aim of this study was to optimize the composition of the resulting photoactive layer in order to tune its spectroscopic properties, *i.e.* broadband absorption in the visible range, and the photosensitizing properties. The deposited layers were characterized by electrochemical and spectroscopic methods. The efficiency of the visible light-driven singlet oxygen photogeneration was tested in the process of α–terpinene oxidation leading to ascaridole formation, that was followed by UV–Vis spectroscopy. Quantum yields of $^1O_2$ production by the investigated layers were estimated with chemical quencher, *i.e.* 1,3–diphenylisobenzofuran (DPBF). The influence of the monomers ratio on the electrochemical, spectroscopic and photoactive properties of the layer was studied.

2. Experimental

2.1. Materials

C_{60}Se dyad and BisSe (Fig. 1) were synthesized applying previously reported procedures [20,30,31]. The synthetic routes and the product identification are given in the Supporting Information. The electrochemical co-deposition of the photoactive layers and their characterization was conducted in Tetrabutylammonium tetrafluoroborate ($TBABF_4$) (Sigma Aldrich, 99%) electrolyte solution in dichloromethane (HPLC grade, Sigma Aldrich). The photosensitizing properties were tested with α-Terpinene (TCI, purity 90%) in acetonitrile (Sigma Aldrich) or 1,3-diphenylisobenzofuran (DPBF) (Acros Organics, purity > 97%) in methanol (Acros Organics, 99.9%). Rose Bengal (Acros Organics) was used as a reference in the determination of the quantum yield of singlet oxygen photogeneration.

2.2. Electrochemical co-deposition of C_{60}Se and BisSe

The electrochemical co-deposition of C_{60}Se and/or BisSe monomers was conducted using SPI-150 electrochemical workstation (Bio-Logic).

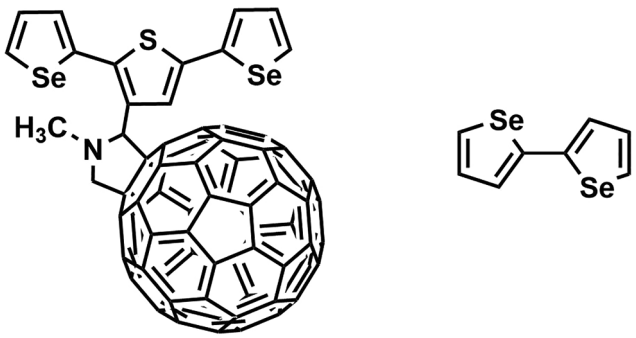

Fig. 1. Investigated monomers: C_{60}Se dyad and BisSe.

A three-electrode cell was used with a platinum disc electrode (Pt, EDAQ, 1 mm dia.) or an Indium-Tin Oxide (ITO)/borosilicate glass (Präzisions Glas & Optik GmbH, PGO) acting as a working electrode, a silver wire - as a pseudoreference electrode and a platinum wire - as a counter electrode. The potential was calibrated with respect to ferrocene (Fc/Fc^+) internal standard. The platinum disc electrode was cleaned with a diamond paste. All electrodes were washed with acetone and dichloromethane and were placed in a Teflon holder in 2 ml conical cell or 5 ml cell, if Pt or ITO were used as a working electrode, respectively. The electrochemical polymerization of C_{60}Se and BisSe was carried out by cyclic voltammetry (CV) within the potential range (-0.6 ; 0.9) V vs Fc/Fc^+ at the scan rate 0.05 V/s in the monomer-containing solution in 0.1 M $TBABF_4$ / dichloromethane. The layer was deposited within 10 scan cycles with the initial anodic polarization. The concentration of C_{60}Se dyad was kept constant at 0.45 mM in all the experiments, while the concentration of BisSe was varied, in order to obtain a different molar ratio of the monomers (5:1, 2:1, 1:1, 1:2 and 1:5). The solution was homogenized with ultrasonic mixing for 15 min and then it was bubbled with Argon (Ar) to remove oxygen prior to measurements.

2.3. Electrochemical and spectroscopic characterization of P(C_{60}Se:BisSe) layers

The electrochemical properties of the layers were investigated in a monomer-free electrolyte solution (0.1 M $TBABF_4$ /CH_2Cl_2 purged with Ar before measurements) using SPI-150 electrochemical workstation (Bio-Logic) and the above-mentioned three-electrode system. CV curves were recorded within (-1.8 ÷ -0.6) V or (-0.6 ÷ 0.9) V vs Fc/Fc^+ potential ranges at 0.05 V/s scan rate.

The content of fullerene in the deposited films was estimated using Equation (1) [32]:

$$\Gamma_{C60} = \frac{Q}{n \bullet F \bullet A} \quad (1)$$

where Q is a charge exchanged in a reversible reduction of C_{60} to $C_{60}^{\bullet -}$, n is a number of electrons, here: equal to 1, A is a platinum electrode surface area (0.785 mm^2) and F is Faraday constant.

Hewlett Packard 8452A UV–Vis spectrometer was used to record UV–Vis spectra of the photoactive layers deposited on ITO and UV–Vis spectra of 0.025 mM solution of C_{60}Se, C_{60} and BisSe in CH_2Cl_2.

IR spectra of the photoactive layers deposited on a platinum plate, powder C_{60}, BisSe and C_{60}Se dyad were collected using ATR mode with Perkin Elmer Spectrum Two IR spectrometer equipped with DTGS MIR detector in the range 2500 – 450 cm^{-1}. Additionally, Raman spectra of co-deposited films were acquired with Renishaw inVia Raman Microscope (Renishaw, Inc., New Mills, UK, with high sensitivity ultra-low noise RenCam CCD detector). A diode laser with the wavelength of 514 nm (maximum power of 12 mW, reduced to 5%), 2400-line/mm grating and 50x objective were used. Renishaw software was applied for spectra smoothing and baseline subtraction.

X-ray photoelectron spectroscopy (XPS) investigations of photoactive layers deposited on ITO utilized an Mg Kα radiation ($h\nu$ = 1253.6 eV), having an overall full width half maximum energy resolution of about 0.9 eV. The spectrometer is a 150 mm hemispherical analyzer from SPECS GmbH working in magnification mode at a pass energy of 20 eV. The samples were mounted on a flat plate with two wing clamps touching the upper part of the specimen, thus ensuring good mechanical and electric contact. Before each experiment, the sample resistance with respect to the ground was checked, the measured resistance was in the range from 5 to 15 Ohm. The fixed samples were placed in an ultra-high vacuum chamber (base pressure of about 1×10^{-10} mbar) [33]. The samples, coming from outside, were firstly inserted inside a fast-entry and, after a couple of hours of pumping, transferred inside the main chamber. No charging effects or sample detriments in vacuum have been detected during the measurements.

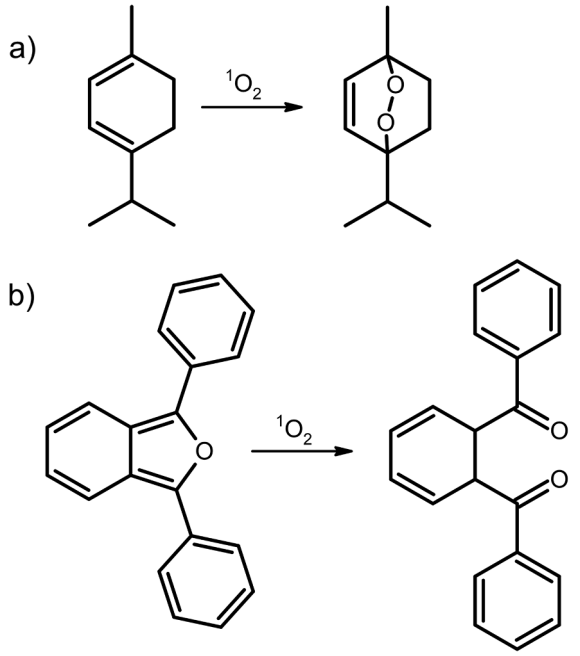

Fig. 2. Scheme of reaction of singlet oxygen with a) α-terpinene and b) DPBF.

2.4. Photogeneration of singlet oxygen by P(C_{60}Se:BisSe) layers

The photogeneration of singlet oxygen molecule was tested with α-terpinene in acetonitrile and 1,3–diphenylisobenzofuran (DPBF) in methanol. The reaction schemes are given in Fig. 2a and Fig. 2b, respectively.

The photosensitizing properties of the deposited layers under visible light illumination were tested with 0.05 mM α-terpinene in acetonitrile. The process was followed *in situ* in 10 × 4 mm quartz cuvette (Hellma Analytics) arranged as a thin layer cell, as in our previous works [20,34]. The setup scheme is given in Fig.S2. The UV–Vis spectra of α-terpinene were collected with Hewlett Packard 8452A UV–Vis spectrometer. Ca. 0.5 cm^2 of sample surface was illuminated with a xenon lamp equipped with a filter transmitting only the radiation above 400 nm, that was placed perpendicularly to the UV–Vis spectra acquisition. The yield and the kinetic parameters of the process were determined based on the decrease in the absorption of α-terpinene at 266 nm [20,34].

DPBF (0.05 mM in CH_3OH) was applied as $^1O_2$ specific quencher under green light illumination. The measurement set-up was arranged as for α-terpinene tests. In this case 532 nm diode laser (Oxxius, LCX-532L-150-CSB-PPA model, 150 mW maximum power, 50 mW power used) was applied as an excitation source. The quantum yields of singlet oxygen photogeneration, Φ, were estimated applying so-called DPBF-method and Rose Bengal (RB) as a reference with known Φ_{RB} equal to 0.80 in CH_3OH. The quantum yield of photochemical production of $^1O_2$ can be calculated using Equation (2).

$$\Phi_i = \Phi_{RB} \cdot \frac{m_i}{m_{RB}} \cdot \frac{\alpha_{RB}}{\alpha_i} \quad (2)$$

where Φ_i and Φ_{RB} are quantum yields of singlet oxygen photogeneration by unknown photosensitizer or RB, respectively; m_i and m_{RB} are rate constants of DPBF oxidation in the presence of an unknown photosensitizer or RB, respectively, and α is absorption correction factor given by $\alpha = 1 - 10^{-A}$ (A is absorbance at irradiation wavelength, here: 532 nm) [35-38].

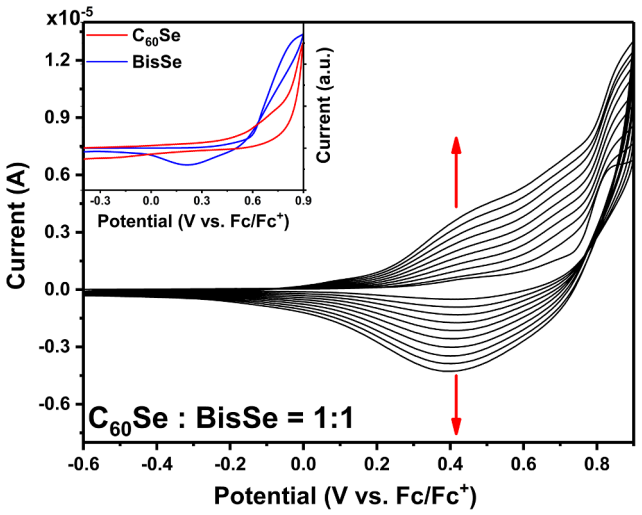

Fig. 3. CV curves recorded for Pt disc electrode in electrolyte solution containing C_{60}Se and BisSe in 1:1 M ratio; arrows indicating the trend of change in the recorded currents. Inset: CV curves recorded for Pt disc electrode in electrolyte solution containing C_{60}Se (red line) or BisSe (blue line).

3. Results and discussion

3.1. Electrochemical co-deposition of C_{60}Se and BisSe

The electrochemical polymerization of monomers was firstly investigated with the platinum disc electrode (Pt). As in our previous works [20,39] such strategy was chosen, since it allows to control the process of layer formation and the amount of the electroactive species being deposited. Fig. 3 presents CV curves recorded during continuous scanning in the equimolar solution of C_{60}Se and BisSe. In the first anodic scan an irreversible oxidation at 0.85 V (vs. Fc/Fc^+) is observed, that can be assigned to the oxidation of organic unit, namely selenophene group, to form radical cations [40]. In the consecutive scans the increase in the recorded current in the broad potential range can be observed, indicating the deposition of the electroactive layer on the platinum electrode surface. Similar CV curves were recorded for ITO acting as a working electrode. The electropolymerization process was conducted only in the anodic domain in order to activate organic units only and to ensure the stability of fullerene present in C_{60}Se monomer. Both, the current increase and the appearance of the new redox couple centered at ca. 0.4 V (vs. Fc/Fc^+), confirm the polymerization of the organic units to form conjugated polymeric layer [41]. It can be seen in the first scan cycle recorded in the single-component solutions (Fig. 3, inset) that the onset of the anodic oxidation, initiating electropolymerization process, is located at ca. 0.4 V (vs. Fc/Fc^+) for both monomers. Therefore, it can be stated that under applied conditions both C_{60}Se and BisSe undergo electrochemical polymerization [42].

3.2. Electrochemical and spectroscopic characterization of P(C_{60}Se:BisSe) layers

3.2.1. Cyclic voltammetry

The electrodeposited polymeric layers, consisting of selenophene and thiophene rings with incorporated fullerene photosensitizers, were in turn characterized by electrochemical and spectroscopic techniques.

The CV curve of P(C_{60}Se_BisSe_1:1) layer recorded in the pure electrolyte solution (Fig. 4) shows three redox couples located at ca. 0.4 V and −1.2 V and −1.5 V vs. Fc/Fc^+. The first signal, that arises from the redox process within the polymeric unit, occurs at potential that lies between the potentials of the corresponding signal in P(C_{60}Se) and P(BisSe) – that is ca. 0.6 V and 0.3 V vs. Fc/Fc^+, respectively. Hence, the presence of both monomer in the structure of the layer is

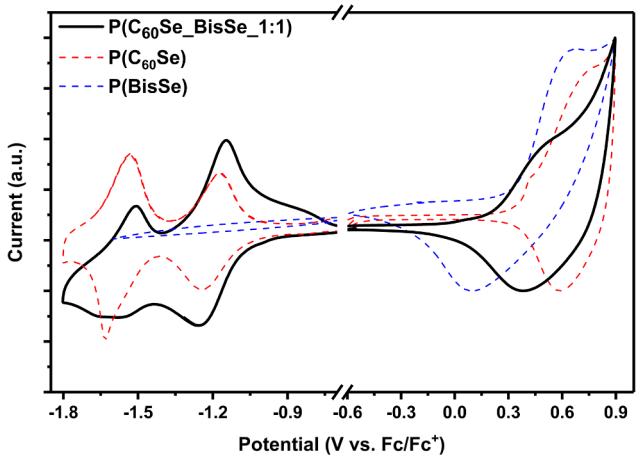

Fig. 4. CV curves recorded for P(C_{60}Se_BisSe_1:1) (black line), P(C_{60}Se) (red dashed line) and P(BisSe) (blue dashed line) deposited on Pt disc electrode in electrolyte solution.

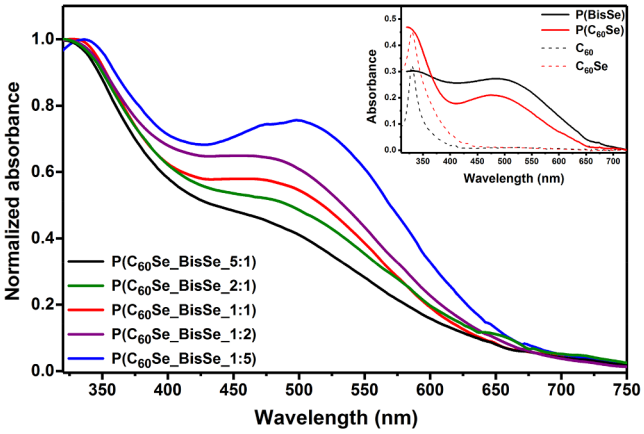

Fig. 5. UV–Vis spectra of P(C_{60}Se_BisSe) layers deposited on ITO from solutions with varied molar ratios of monomers. Inset: UV–Vis spectra of 0.025 mM solution of C_{60} (black dashed line), C_{60}Se in dichloromethane (red dashed line), P(C_{60}Se) (red line) and P(BisSe) (black line) layers deposited on ITO.

confirmed.

In the cathodic scan, two reversible redox couples centered at ca. −1.2 V and at ca. −1.5 V vs. Fc/Fc^+ are observed. Those signals, which are absent in the case of P(BisSe) layer, arise from the two-step reduction of C_{60} to $C_{60}^{\bullet-}$ and then to C_{60}^{2-}, respectively [40,43]. This confirms the presence of fullerene units in P(C_{60}Se_BisSe_1:1) layer. Similar CV curves were recorded for other polymeric films deposited from the solution with varied monomers ratio. Taking into account the area under first reduction peak arising from C_{60} to $C_{60}^{\bullet-}$ transition, the fullerene content in the formed layers was roughly estimated. As expected, the amount of C_{60} units in P(C_{60}Se_BisSe) films was decreasing by lowering the C_{60}Se – to – BisSe ratio in the feed solution (Table 1).

3.2.2. UV–Vis spectroscopy

The UV–Vis spectra of the electrochemically deposited layers (Fig. 5) show two distinctive absorption bands. The band with maximum at 330 nm corresponds to the fullerene absorption, that for pristine C_{60} in CH_2Cl_2 solution is located at 329 nm (Fig. 5, inset). The second band present in the low energy region can be linked to the absorption of conjugated polymeric unit, namely π → π* transition. The UV–Vis spectrum of the fullerene-dyad monomer shows only one broad signal covering C_{60} and organic unit absorption (Fig. 5, inset), while in the UV–Vis spectra of P(C_{60}Se_BisSe) layers the band of selenophene/thiophene-containing matrix is batochromicaly shifted and well-separated from the C_{60} absorption band, which confirms that electrodeposition process results in the elongation of the conjugate organic chain [44]. The maximum of the above-mentioned band is located at ca. 490 nm and is slightly red-shifting with the increase in the BisSe content. In all cases, only one absorption maximum is observed in the visible region and it is located between the maxima of the corresponding homopolymers, *i.e.* 480 nm for P(C_{60}Se) and 500 nm for P(BisSe) (Fig. 5, inset). This may indicate that the electrochemical codeposition results in the formation of the copolymeric structure rather than the blend of homopolymers [45,46]. Since the onset of π-π*

Table.1
Fullerene content in P(C_{60}Se_BisSe) layers deposited from the solution with various molar ratio of monomers.

Photoactive layer	Fullerene content [mol/mm^2]
P(C_{60}Se_BisSe_5:1)	$5.7 \cdot 10^{-9}$
P(C_{60}Se_BisSe_2:1)	$4.2 \cdot 10^{-9}$
P(C_{60}Se_BisSe_1:1)	$2.5 \cdot 10^{-9}$
P(C_{60}Se_BisSe_1:2)	$1.2 \cdot 10^{-9}$
P(C_{60}Se_BisSe_1:5)	$4.9 \cdot 10^{-11}$

transition band is located at ca. 675 nm for all the films, it can be stated that the resulting photoactive layers possess comparable effective conjugation length [47]. Importantly, the absorbance in the Vis range is significantly increasing with respect to C_{60} absorption at 330 nm, with the increase in the content of BisSe. This confirms that the spectroscopic properties of the photoactive layer can be tuned by changing the monomers ratio in the feed solution.

3.2.3. ATR-IR spectroscopy

Fig. 6 presents the IR spectra of both monomers and P(C_{60}Se_BisSe_1:1) layer recorded in the ATR mode. In the case of fullerene dyad spectrum, four characteristic C_{60} bands are observed at 524 cm^{-1}, 574 cm^{-1}, 1177 cm^{-1} and 1427 cm^{-1}, that can be assigned to the vibrations of pentagons and hexagons of the fullerene cage [48]. The presence of organic unit in the monomer dyad is confirmed by C-H out-of-plane vibrations of the monosubstituted selenophene ring located at 678 cm^{-1} [47]. The latter vibration is the most dominant in the IR spectrum of BisSe, together with the aromatic stretching band at 1427 cm^{-1} [47] and other signals in the fingerprint region at 748 cm^{-1} and 814 cm^{-1}, that can be assigned to the adjacent and isolated out-of-plane bending vibrations of the selenophene ring [49]. For P(C_{60}Se_BisSe_1:1) layer the aromatic stretching vibrations, namely

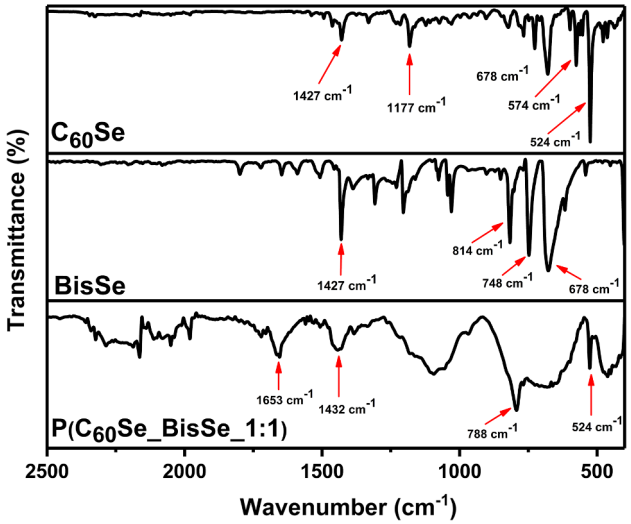

Fig. 6. ATR-IR spectra of C_{60}Se, BisSe and P(C_{60}Se_BisSe_1:1) layer deposited on Pt plate.

symmetric and asymmetric stretching of C = C in the selenophene ring, are observed at 1432 cm^{-1} and 1653 cm^{-1}, respectively [50]. Those bands are significantly broaden when compared to monomers spectra, which is typical for electrodeposited polymeric layers [44]. The effectiveness of the electropolymerization process is also confirmed by the decrease in the relative intensity of 678 cm^{-1} band being specific for the monosubstituted heterocyclic ring. The strong signal at 788 cm^{-1} arises from C-H out-of-plane vibrations in the 2,5-disubstituted selenophene rings, which indicates that the electrochemical polymerization occurs *via* α,α'-mechanism [51]. This is also supported by the absence of the band at ca. 820 cm^{-1} that is characteristic for polyselenophene obtained by α,β-coupling [50]. Moreover, the band located at 524 cm^{-1} confirms the presence of C_{60} units in the deposited photoactive polymeric layer. The position of the vibrations of the fullerene spheres, *i.e.* "pentagonal pinch" A_g mode, in the recorded Raman spectra (Fig. S3) gives the final check of the structure of the formed layer. The mentioned band is located at slightly lower wavenumbers (1455 cm^{-1}) than for the pristine C_{60}, but this can be a result of the additional contribution of the C = C stretching vibration of BisSe, rather than the oligomerization of the fullerene units [52,53].

3.2.4. X-ray photoelectron spectroscopy

The structures of the electrochemically polymerized photoactive layers were further investigated by XPS (Fig. 7). In the survey spectra obtained for P(C_{60}Se_BisSe_1:1)/ITO layer, given in Fig. 6a, signals of Se 3*d*, S 2*p*, C 1 *s* and N 1 *s* appear at 56 eV, 165 eV, 286 eV and 399 eV, respectively [54,55]. While the presence of selenium, sulfur and nitrogen is specific for the deposited layer, the carbon signal arises from the deposited layer and the so-called adventitious carbon residues [56,57]. The O 1 *s* peak, placed at around 530 eV, has reasonably the same origin, even if the ITO substrate contribution cannot be excluded. Importantly, only weak signals coming from the electrolyte or solvent used during the electrodeposition process, like F 1 *s* at 686 eV, are observed. Similarly, only low-intensity peaks from the ITO substrate are recorded, *i.e.* Sn 3*d* at 485 eV, In 3*d* at 444 eV and Si 2*p* at 100 eV [58], which confirms the homogeneity of the layer.

The high-resolution spectra recorded for P(C_{60}Se_BisSe_1:1) are shown in Fig. 7b – d. The experimental data (dashed lines) were fitted using CASA XPS with components given as a product of Gaussian and Lorentzian lines. The Shirley function was used for the background subtraction [20,59]. The decomposition of N 1 *s* region (Fig. 7b) gives one component at 399.4 eV arising from the amine-linker in the fullerene-organic dyad [60]. In the case of two partially overlapping regions, namely S 2*p* and Se 3*p* region (Fig. 7c) four components, *i.e.* Se $3p_{3/2}$ and S $2p_{3/2}$ with their spin–orbit split counterparts can be distinguished at 162.3 eV and 163.9 eV, respectively [54,55,61]. Moreover, for Se 3*d* region (Fig. 7d) two spin–orbit components Se $3d_{5/2}$ and Se $3d_{3/2}$ with 0.86 eV separation and ca. 1.4-ratio are observed [62,63]. The position of both S $2p_{3/2}$ and Se $3d_{5/2}$ confirms the presence of thiophene- and selenophene-containing organic layer on the ITO surface. Importantly, since no additional components are observed in S 2*p* or Se 3*d* regions, it can be stated that no oxidized species are present within 2–3 nm from the sample surface [55,61]. The analysis of the C 1 *s* spectrum (Fig.S4) reveals the presence of five components arising from both - the deposited layer and the adventitious carbon [64]. The ratio between the components (Tab.S1) is in good agreement with the stoichiometry of the layer, confirming that the contamination is not significant.

Taking into account that N 1 s signal recorded at 399.4 eV arises from the amine-linker that is present only in the C_{60}Se dyad, the high-

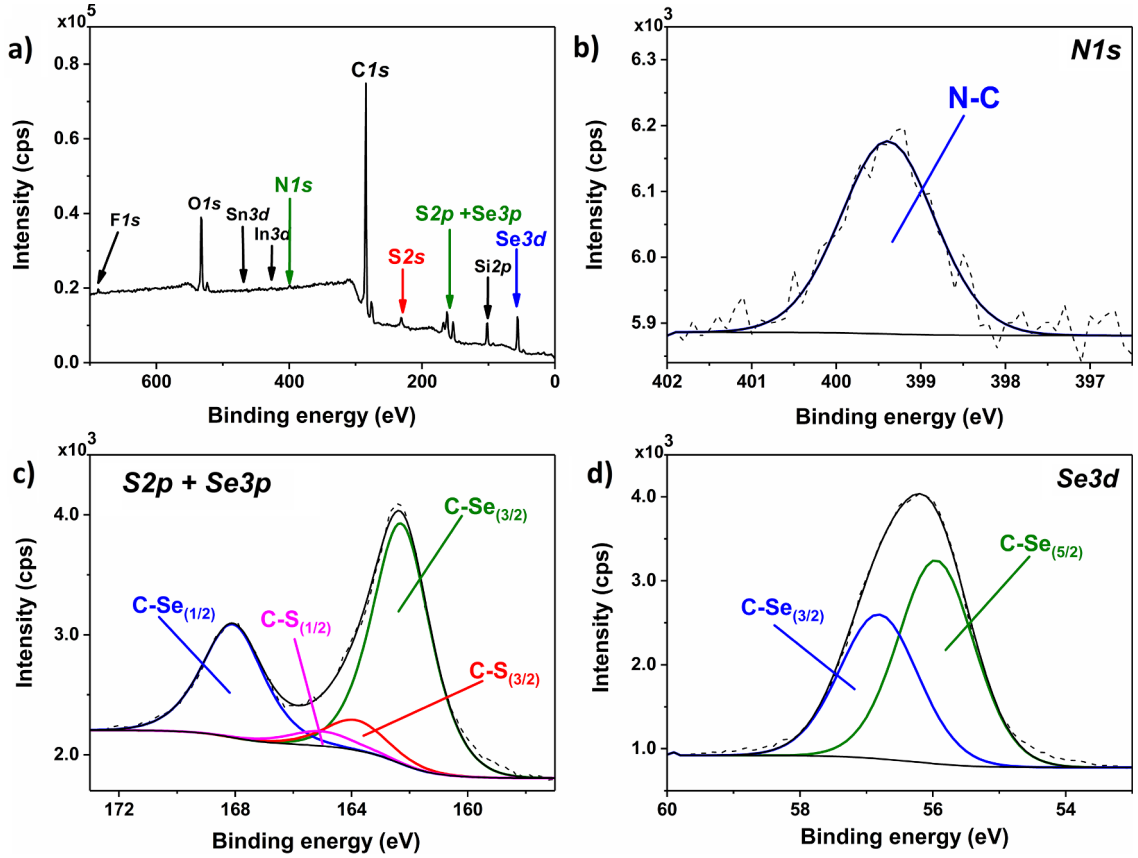

Fig. 7. XPS a) wide scan (pass energy 40 eV) and high resolution spectra b) N 1 s, c) S 2p + Se 3p and d) Se 3d recorded for P(C_{60}Se_BisSe_1:1) layer deposited on ITO.

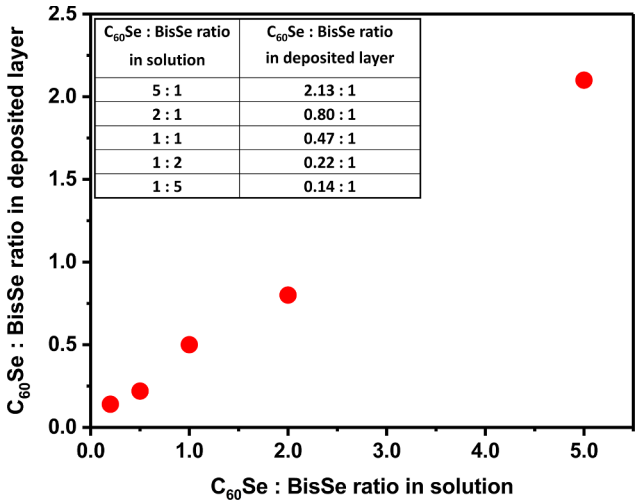

Fig. 8. Composition of photoactive layer as a function of monomers ratio in feed solution.

resolution N 1 *s* and Se 3*d* regions after correcting the signal intensity for the element and the transition specific photoemission cross sections, were in turn used to estimate the composition of the deposited P(C_{60}Se_BisSe) layers. Fig. 8 presents the relation between the composition of the feed solution and the monomers ratio in the resulting layer. As assumed, the monomers ratio in the solution strongly influences the deposited layer composition: the increase in the concentration of the fullerene-containing monomer yields layers with higher C_{60} content, with almost linear relation. This is in agreement with the above-mentioned CV and UV–Vis spectroscopy results. The estimated monomers ratios in the deposited layers are not equal to the ones in the feed solutions. The significantly higher content of BisSe units was observed, which suggests that, though both monomers undergo irreversible oxidation at similar potentials, the electropolymerization of BisSe monomer is more effective, probably because of the steric effect.

3.3. Singlet oxygen photogeneration by P(C_{60}Se:BisSe) layers

The photogeneration of singlet oxygen in homogenous and heterogeneous systems can be investigated directly, *i.e.* by measuring luminesce at ca. 1270 nm, or indirectly with chemical traps. Since the emission signal of singlet oxygen is quite weak, the second strategy is more common. Various chemical traps that can be monitored with UV–Vis or EPR spectroscopies have been proposed for the indirect detection of $^1O_2$ [65,66]. In this work, α-terpinene was used for the investigation of visible light photogeneration of ROS, while DPBF – specific singlet oxygen quencher, was applied under green-light illumination for the determination of the quantum yield.

The effectiveness of the visible light-induced photooxidation reaction was monitored by UV–Vis spectroscopy as the decrease in the absorption of α-terpinene at 266 nm [20]. Fig. 9a presents the UV–Vis spectra of α-terpinene recorded during illumination of P(C_{60}Se_BisSe_1:1) layer with the xenon lamp equipped with the filter transmitting only visible radiation. The decrease in the characteristic absorption band of α-terpinene observed at 266 nm indicates its reaction with ROS photogenerated by P(C_{60}Se_BisSe_1:1) layer. The photooxidation of α-terpinene results in the formation of ascaridole (Fig. 2a) [16,67]. Importantly, the deposited layer is not dissolving in the reaction medium, since no new bands are observed in the recorded spectra during the photoprocess.

Fig. 9b shows that almost no decrease in the substrate absorbance is observed when unmodified ITO is illuminated, which confirms that under applied conditions the process of α-terpinene self-decomposition can be excluded. Additionally, the decrease in the absorbance after 30 min of illumination is significantly higher for the electrochemically deposited polymeric layer containing fullerenes than for the layer containing only BisSe monomer. Thus, it can be stated that incorporated C_{60} photosensitizers are mainly responsible for the ROS photogeneration. As in our previous work, it is shown that the photosensitizers based on carbon nanostructures retain their photoactivity after deposition on a solid support [34].

The activity of P(C_{60}Se_BisSe_1:1) layer towards singlet oxygen was also tested applying DPBF - chemical quencher and 532 nm laser as an illumination source. Fig. S5 presents the UV–Vis spectra of DPBF in methanol recorded during irradiation of P(C_{60}Se_BisSe_1:1) layer with the green laser. The drop in the DPBF absorbance at 410 nm confirms that the energy transfer from the poly(selenophene) matrix to C_{60} can occur and it may result in the formation of $^1O_2$ species [4,6,7,68-71]. The quantum yield of singlet oxygen photogeneration was determined by the DPBF-method with Rose Bengal as a reference [36-38]. Φ is equal to ca. 0.7% for P(C_{60}Se_BisSe_1:1) and P(C_{60}Se) layers, suggesting that the efficiency of the above-mentioned energy transfer is comparable in both cases, even if the additional organic-only component (BisSe) acting mainly as a visible light antenna, is introduced into the deposited layer.

Further, as presented in Fig. 9b, the drop in α-terpinene absorbance at 266 nm is ca. 2.5-times higher for P(C_{60}Se_BisSe_1:1) layer than for the layer consisting of the fullerene dyad only - P(C_{60}Se). This can be explained by higher absorbance of the photoactive layer containing BisSe units in the visible range, which confirms the effectiveness of the assumed strategy.

In the next step, all electrochemically co-deposited layers were applied as a source of $^1O_2$ in the oxidation of α-terpinene, yielding similar set of spectra as presented in Fig. 9a. In order to compare the efficiency of the photoprocess, the rate constants were determined based on the drop of α-terpinene concentration. Assuming the pseudo-zero order kinetics [20], the rate constants were estimated with a linear regression as a slope of the line (c-$c_{initial}$) vs. time. As it can be seen in Table 2, the highest value of the rate constant was observed for the polymeric layer deposited from the feed solution with monomers ratio equal to 1. Further increase in the content of the organic unit or fullerene-dyad resulted in the drop of the reaction rate. This indicates that the ratio between the fullerene photosensitizer and the poly(selenophene) matrix, acting as an antenna for visible light, is the best optimized in the case of P(C60Se_BisSe_1:1) layer.

4. Conclusions

In the presented work, C_{60}Se fullerene-dyad was electrochemically co-deposited with bis-selenophene on Pt or ITO/glass, yielding the polymeric matrix with incorporated C_{60} photosensitizers. The proposed strategy resulted in the formation of the thin photoactive layer, which structure was confirmed with electrochemical and spectroscopic techniques. It was shown that the composition of the resulting layer can be simply varied by changing the monomers ratio in the feed solution. This, in turn, allows to tune the spectroscopic properties, namely the absorption in the visible range, and the photosensitizing properties of the deposited films. It was found that the layer with ca. 1:2 ratio between the fullerene dyad and bis-selenophene units, formed from the equimolar solution, shows the highest efficiency of singlet oxygen photogeneration under visible light illumination. The quantum yield of the photoprocess was comparable for C_{60}Se_BiSe and C_{60}Se-only layers. The presented results demonstrate that the efficiency of the visible light photogeneration can be simply enhanced by the introduction of the visible light-harvesting organic units into fullerene-containing photoactive layer.

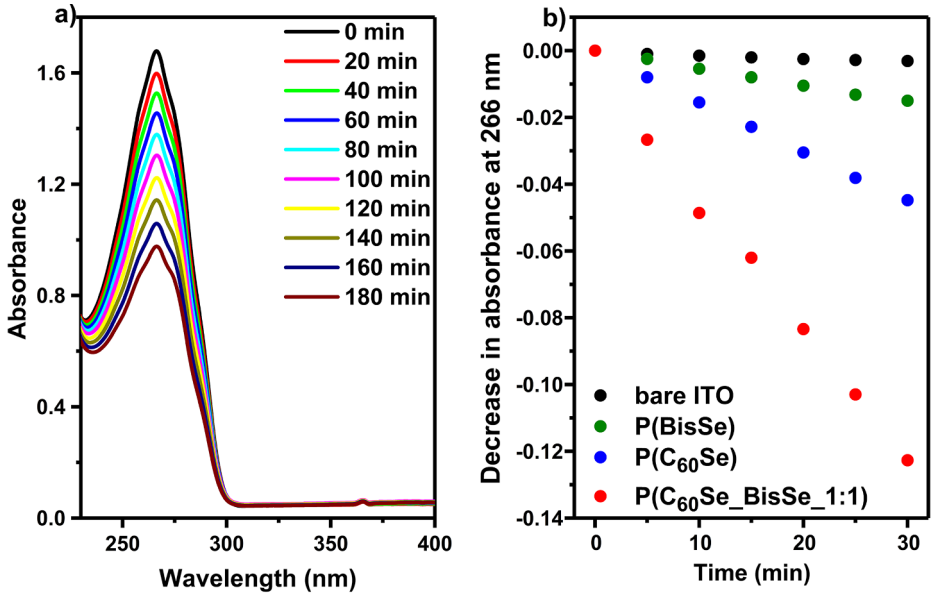

Fig. 9. a) UV–Vis spectra of α-terpinene recorded during illumination of P(C60Se_BisSe_1:1) layer with xenone lamp equipped with filter transmitting > 400 nm, b) decrease in the absorbance of α-terpinene at 266 nm during illumination of P(C60Se_BisSe_1:1), P(BisSe), P(C60Se) layers deposited on ITO and unmodified ITO.

Table.2
Rate constants of α-terpinene photooxidation reaction with singlet oxygen generated by P(C_{60}Se_BisSe) layers with various composition.

Photoactive layer	k [$mM^{-1}min^{-1}$]
P(C_{60}Se_BisSe_5:1)	(1.72 ± 0.01)·10^{-4}
P(C_{60}Se_BisSe_2:1)	(2.85 ± 0.01)·10^{-4}
P(C_{60}Se_BisSe_1:1)	(5.10 ± 0.02)·10^{-4}
P(C_{60}Se_BisSe_1:2)	(2.52 ± 0.01)·10^{-4}
P(C_{60}Se_BisSe_1:5)	(1.30 ± 0.01)·10^{-4}
P(C_{60}Se)	(2.03 ± 0.01)·10^{-4}

CRediT authorship contribution statement

Aleksandra Nyga: Investigation, Visualization. **Radoslaw Motyka:** Investigation. **Gianlorenzo Bussetti:** Investigation, Formal analysis, Writing - review & editing. **Alberto Calloni:** Investigation, Formal analysis. **Madan Sangarashettyhalli Jagadeesh:** Investigation. **Sylwia Fijak:** Investigation. **Sandra Pluczyk-Malek:** Validation, Writing - review & editing. **Przemyslaw Data:** Supervision, Funding acquisition. **Agata Blacha-Grzechnik:** Conceptualization, Methodology, Investigation, Formal analysis, Visualization, Writing - original draft, Writing - review & editing.

Acknowledgements

This work was supported by National Science Center, Poland (grand number: 2016/21/D/ST5/01641). A.N. & P.D. kindly acknowledge the support received from the First Team program of the Foundation for Polish Science co-financed by the European Union under the European Regional Development Fund (project number: First TEAM POIR.04.04.00-00-4668/17-00).

Appendix A. Supplementary data

Supplementary data (Synthesis and spectroscopic characterization of C_{60}Se and BisSe monomers. Scheme of setup for *in-situ* investigation of singlet oxygen photogeneration. Raman spectra of P(BisSe) and P(C_{60}Se:BisSe) layers. XPS high resolution spectrum C1s recorded for P(C_{60}Se_BisSe_1:1) layer deposited on ITO. UV–Vis spectra of DPBF recorded during illumination of P(C_{60}Se_BisSe_1:1) layer with 532 nm diode laser.) to this article can be found online at https://doi.org/10.1016/j.apsusc.2020.146594.

References

[1] J. Wahlen, D.E. de Vos, P.A. Jacobs, L. Alsters, Solid Materials as Sources for Synthetically Useful Singlet Oxygen, Adv. Synth. Catal. 346 (2004) 152–164, https://doi.org/10.1002/adsc.200303224.
[2] J. Wang, H. Huang, Z. Xu, J. Kou, C. Lu, The Potential of Carbon-based Materials for Photocatalytic Application The Potential of Carbon-based Materials for Photocatalytic Application, Curr. Org. Chem. 18 (2014) 1346–1364, https://doi.org/10.2174/1385272819666140424214022.
[3] F. Prat, R. Stackow, R. Bernstein, W. Qian, Y. Rubin, C.S. Foote, Triplet-State Properties and Singlet Oxygen Generation in a Homologous Series of Functionalized Fullerene Derivatives, J. Phys. Chem. A. 103 (1999) 7230–7235, https://doi.org/10.1021/jp991237o.
[4] B. Vileno, A. Sienkiewicz, M. Lekka, A. Kulik, L. Forro, In vitro assay of singlet oxygen generation in the presence of water-soluble derivatives of C60, Carbon N. Y. 42 (2004) 1195–1198, https://doi.org/10.1016/j.carbon.2003.12.042.
[5] T. Hamano, K. Okuda, T. Mashino, M. Hirobe, K. Arakane, A. Ryu, Singlet oxygen production from fullerene derivatives : effect of sequential functionalization of the fullerene core, Chem. Commun. (1997) 21–22, https://doi.org/10.1039/A606335G.
[6] L. Huang, X. Cui, B. Therrien, J. Zhao, Energy-Funneling-Based Broadband Visible-Light-Absorbing Bodipy–C60 Triads and Tetrads as Dual Functional Heavy-Atom-Free Organic Triplet Photosensitizers for Photocatalytic Organic Reactions, Chem. - A Eur. J. 19 (2013) 17472–17482, https://doi.org/10.1002/chem.201302492.
[7] Y. Wei, M. Zhou, Q. Zhou, X. Zhou, S. Liu, S. Zhang, B. Zhang, Triplet-triplet Annihilation Upconversion Kinetics of C60-Bodipy Dyads as Organic Triplet Photosensitizers, Phys. Chem. Chem. Phys. 33 (2017) 8689–8691, https://doi.org/10.1039/C7CP03840B.
[8] W. Wu, J. Zhao, J. Sun, S. Guo, Light-Harvesting Fullerene Dyads as Organic Triplet Photosensitizers for Triplet − Triplet Annihilation Upconversions, J. Org. Chem. 77 (2012) 5305–5312, https://doi.org/10.1021/jo300613g.
[9] M.C. DeRosa, R.J. Crutchley, Photosensitized singlet oxygen and its applications, Coord. Chem. Rev. 233–234 (2002) 351–371, https://doi.org/10.1016/S0010-8545(02)00034-6.
[10] S. Nonell, C. Flors, Singlet Oxygen: Applications in Biosciences and Nanosciences, Royal Society of Chemistry (2016), https://doi.org/10.1039/9781782622208.
[11] M.S. Baptista, J. Cadet, P. Di Mascio, A.A. Ghogare, A. Greer, M.R. Hamblin, C. Lorente, S.C. Nunez, M. Sim, H. Thomas, M. Vignoni, T.M. Yoshimura, Type I and Type II Photosensitized Oxidation Reactions : Guidelines and Mechanistic Pathways, Photochem. Photobiol. 93 (2017) 912–919, https://doi.org/10.1111/php.12716.
[12] H. Zou, F. Jin, X. Song, J. Xing, Singlet oxygen generation of photosensitizers effectively activated by Nd3+-doped upconversion nanoparticles of luminescence intensity enhancing with shell thickness decreasing, Appl. Surf. Sci. 400 (2017) 81–89, https://doi.org/10.1016/j.apsusc.2016.12.174.
[13] P.R. Ogilby, Singlet oxygen : there is indeed something new under the sun, Chem. Soc. Rev. 39 (2010) 3181–3209, https://doi.org/10.1039/b926014p.

[14] P.R. Ogilby, C.S. Foote, Chemistry of Singlet Oxygen. 42. Effect of solvent, Solvent Isotopic Substitution, and Temperature on the Lifetime of Singlet Molecular Oxygen, J. Am. Chem. Soc. 105 (1983) 3423–3430, https://doi.org/10.1021/ja00349a007.

[15] K.I. Salokhiddinov, I.M. Bytev, G.P. Gurinovich, Lifetime of singlet oxygen in various solvents, J. Appl. Scpectroscopy. 34 (1981) 561–564, https://doi.org/10.1007/bf00613067.

[16] J. Kyriakopoulos, M.D. Tzirakis, G.D. Panagiotou, M.N. Alberti, K.S. Triantafyllidis, S. Giannakaki, K. Bourikas, C. Kordulis, M. Orfanopoulos, A. Lycourghiotis, Highly active catalysts for the photooxidation of organic compounds by deposition of [60] fullerene onto the MCM-41 surface : A green approach for the synthesis of fine chemicals, Appl. Catal. B, Environ. 117–118 (2012) 36–48. doi:10.1016/j.apcatb.2011.12.024.

[17] S. Guo, H. Zhang, L. Huang, Z. Guo, G. Xiong, J. Zhao, Porous material-immobilized iodo-Bodipy as an efficient photocatalyst for photoredox catalytic organic reaction to prepare pyrrolo[2,1- a]isoquinoline, Chem. Commun. 49 (2013) 8689–8691, https://doi.org/10.1039/c3cc44486d.

[18] M. Condat, J. Babinot, S. Tomane, J.-P. Malval, I.-K. Kang, F. Spillebout, P.-E. Mazeran, J. Lalevee, S.A. Andalloussi, D.-L. Versace, Development of photo-activable glycerol-based coatings containing quercetin for antibacterial, RSC Adv. 6 (2016) 18235–18245, https://doi.org/10.1039/c5ra25267a.

[19] C. Piccirillo, S. Perni, J. Gil-Thomas, P. Prokopovich, M. Wilson, J. Pratten, I.P. Parkin, Antimicrobial activity of methylene blue and toluidine blue O covalently bound to a modified silicone polymer surface, J. Mater. Chem. 34 (2009) 6167–6171, https://doi.org/10.1039/b905495b.

[20] A. Blacha-Grzechnik, M. Krzywiecki, R. Motyka, Electrochemically Polymerized Terthiopehene − C60 Dyads for the Photochemical Generation of Singlet Oxygen, J. Phys. Chem. C. 123 (2019) 25915–25924, https://doi.org/10.1021/acs.jpcc.9b06101.

[21] S. Ren, M. Bernardi, R.R. Lunt, V. Bulovic, J.C. Grossman, S. Gradecak, Toward Efficient Carbon Nanotube / P3HT Solar Cells: Active Layer Morphology, Electrical and Optical Properties, Nano Lett. 11 (2011) 5316–5321, https://doi.org/10.1021/nl202796u.

[22] D. Meng, D. Sun, C. Zhong, T. Liu, B. Fan, L. Huo, Y. Li, W. Jiang, H. Choi, T. Kim, J.Y. Kim, Y. Sun, Z. Wang, A.J. Heeger, High-Performance Solution-Processed Non-Fullerene Organic Solar Cells based on Selenophene-Containing Perylene Bisimide Acceptor, J. Am. Chem. Soc. 138 (2016) 375–380, https://doi.org/10.1021/jacs.5b11149.

[23] Y. Lin, J. Wang, Z. Zhang, H. Bai, Y. Li, D. Zhu, X. Zhan, An Electron Acceptor Challenging Fullerenes for Efficient Polymer Solar Cells, Adv. Mater. 27 (2015) 1170–1174, https://doi.org/10.1002/adma.201404317.

[24] L. Zhong, H. Bin, I. Angunawela, Z. Jia, B. Qiu, C. Sun, X. Li, Z. Zhang, H. Ade, Y. Li, Effect of Replacing Thiophene by Selenophene on the Photovoltaic Performance of Wide Bandgap Copolymer Donors, Macromolecules. 52 (2019) 4776–4784, https://doi.org/10.1021/acs.macromol.9b00484.

[25] N. Grossiord, J.M. Kroon, R. Andriessen, P.W.M. Blom, Degradation mechanisms in organic photovoltaic devices, Org. Electron. 13 (2012) 432–456, https://doi.org/10.1016/j.orgel.2011.11.027.

[26] B.R. Pacios, A.J. Chatten, K. Kawano, J.R. Durrant, D.D.C. Bradley, J. Nelson, Effects of Photo-oxidation on the Performance of Poly[2-methoxy-5-(3',7'-dimethyloctyloxy)-1,4-phenylene vinylene]:[6,6] -PhenylC61-Butyric Acid Methyl Ester Solar Cells, Adv. Funct. Mater. 16 (2006) 2117–2126, https://doi.org/10.1002/adfm.200500714.

[27] M. Bregnhøj, M. Prete, V. Turkovic, A.U. Petersen, M.B. Nielsen, M. Madsen, P.R. Ogilby, Oxygen-dependent photophysics and photochemistry of prototypical compounds for organic photovoltaics: inhibiting degradation initiated by singlet oxygen at a molecular level, Methods Appl. Fluoresc. 8 (2020) 14001, https://doi.org/10.1088/2050-6120/ab4edc.

[28] A. Tournebize, M. Seck, A. Vincze, A. Distler, H. Egelhaaf, C.J. Brabec, A. Rivaton, H. Peisert, T. Chassé, Solar Energy Materials & Solar Cells Photodegradation of Si-PCPDTBT : PCBM active layer for organic solar cells applications : A surface and bulk investigation, Sol. Energy Mater. Sol. Cells. 155 (2016) 323–330, https://doi.org/10.1016/j.solmat.2016.06.026.

[29] A. Distler, P. Kutka, T. Sauermann, H. Egelhaaf, D.M. Guldi, D. Di Nuzzo, S.C.J. Meskers, R.A.J. Janssen, Effect of PCBM on the Photodegradation Kinetics of Polymers for Organic Photovoltaics, Chem. Mater. 24 (2012) 4397–4405, https://doi.org/10.1021/cm302623p.

[30] P. Data, M. Lapkowski, R. Motyka, J. Suwinski, Electrochimica Acta Influence of heteroaryl group on electrochemical and spectroscopic properties of conjugated polymers, Electrochim. Acta. 83 (2012) 271–282, https://doi.org/10.1016/j.electacta.2012.08.020.

[31] J.P. Parrish, V.L. Flanders, R.J. Floyd, K.W. Jung, Mild and efficient formation of symmetric biaryls via Pd (II) catalysts and Cu (II) oxidants, Tetrahedron Lett. 42 (2001) 7729–7731, https://doi.org/10.1016/S0040-4039(01)01691-4.

[32] D. Bonifazi, O. Enger, F. Diederich, Supramolecular [60] fullerene chemistry on surfaces, Chem. Soc. Rev. 36 (2007) 390–414, https://doi.org/10.1039/b604308a.

[33] G. Berti, A. Calloni, A. Brambilla, G. Bussetti, L. Duò, F. Ciccacci, Direct observation of spin-resolved full and empty electron states in ferromagnetic surfaces, Rev. Sci. Instrum. 85 (2014) 073901, , https://doi.org/10.1063/1.4885447.

[34] A. Blacha-Grzechnik, K. Piwowar, T. Zdyb, M. Krzywiecki, Formation of poly(Azure A) -C60 photoactive layer as a novel approach in the heterogeneous photogeneration of singlet oxygen, Appl. Surf. Sci. 457 (2018) 221–228, https://doi.org/10.1016/j.apsusc.2018.06.262.

[35] F. Lv, Y. Yu, E. Hao, C. Yu, H. Wang, L. Jiao, Highly Regioselective α -Formylation and α -Acylation of BODIPY Dyes via Tandem Cross-Dehydrogenative Coupling with in situ Deprotection, Org. Biomol. Chem. (2019) 1–44, https://doi.org/10.1016/j.cclet.2019.08.004.

[36] C.R. Lambert, I.E. Kochevar, Does Rose Bengal Triplet Generate Superoxide Anion ? J. Am. Chem. Soc. 118 (1996) 3297–3298, https://doi.org/10.1021/ja9600800.

[37] M.I. Burguete, F. Galindo, R. Gavara, S.V. Luis, M. Moreno, D.A. Russell, Singlet oxygen generation using a porous monolithic polymer supported photosensitizer : potential application to the photodynamic destruction of melanoma cells, Photochem. Photobiol. Sci. 8 (2009), https://doi.org/10.1039/b810921d.

[38] N. Epelde-Elezcano, V. Martinez-Martinez, E. Pena-Cabrera, C.F.A. Gomez-Duran, I.L. Arbeloa, S. Lacombe, Modulation of singlet oxygen generation in halogenated BODIPY dyes by substitution at their meso position : towards a solvent-independent standard in the vis region, RSC Adv. 6 (2016) 41991–41998, https://doi.org/10.1039/c6ra05820e.

[39] K. Piwowar, A. Blacha-Grzechnik, R. Turczyn, J. Zak, Electropolymerized phenothiazines for the photochemical generation of singlet oxygen, Electrochim. Acta. 141 (2014) 182–188, https://doi.org/10.1016/j.electacta.2014.07.052.

[40] J. Chen, G. Tsekouras, D.L. Officer, P. Wagner, C.Y. Wang, C.O. Too, G.G. Wallace, Novel fullerene-functionalised poly(terthiophenes), J. Electroanal. Chem. 599 (2007) 79–84, https://doi.org/10.1016/j.jelechem.2006.09.007.

[41] S. Pluczyk, W. Kuznik, M. Lapkowski, R.R. Reghu, J.V. Grazulevicius, The effect of the linking topology on the electrochemical and spectroelectrochemical properties of carbazolyl substituted perylene bisimides, Electrochim. Acta. 135 (2014) 487–494, https://doi.org/10.1016/j.electacta.2014.05.057.

[42] S. Pluczyk, P. Zassowski, C. Quinton, P. Audebert, V. Alain-Rizzo, M. Lapkowski, Unusual Electrochemical Properties of the Electropolymerized Thin Layer Based on a s-Tetrazine-Triphenylamine Monomer, J. Phys. Chem. C. 120 (2016) 4382–4391, https://doi.org/10.1021/acs.jpcc.5b11555.

[43] M. Czichy, P. Wagner, M. Lapkowski, D.L. Officer, Effect of π -conjugation on electrochemical properties of poly (terthiophene)s 3'-substituted with fullerene C60, J. Electroanal. Chem. 772 (2016) 103–109, https://doi.org/10.1016/j.jelechem.2016.04.009.

[44] B. Lu, S. Zhen, S. Ming, J. Xu, G. Zhao, RSC Advances (2015) 70649–70660, https://doi.org/10.1039/c5ra11849b.

[45] M. Ak, H. Ceti, L. Toppare, Blend or copolymer ? Spectroelectrochemical evidence of copolymerization and blending of two electrochromic monomers, Colloid Polym. Sci. 291 (2013) 767–772, https://doi.org/10.1007/s00396-012-2787-7.

[46] R. Holze, Copolymers — A refined way to tailor intrinsically conducting polymers, Electrochim. Acta. 56 (2011) 10479–10492, https://doi.org/10.1016/j.electacta.2011.04.013.

[47] B. Dong, Y. Xing, J. Xu, L. Zheng, J. Hou, F. Zhao, Electrosyntheses of free-standing and highly conducting polyselenophene films in an ionic liquid, Electrochim. Acta. 53 (2008) 5745–5751, https://doi.org/10.1016/j.electacta.2008.03.049.

[48] G. Rambabu, S.D. Bhat, Sulfonated fullerene in SPEEK matrix and its impact on the membrane electrolyte properties in direct methanol fuel cells, Electrochim. Acta. 176 (2015) 657–669, https://doi.org/10.1016/j.electacta.2015.07.045.

[49] C.Y. Park, Y.J. Kim, H.J. Lim, J.H. Park, M.J. Kim, S.W. Seo, C.P. Park, RSC Advances (2015) 4233–4237, https://doi.org/10.1039/C4RA12965B.

[50] J. Xu, J. Hou, S. Zhang, G. Nie, S. Pu, L. Shen, Q. Xiao, Electrosyntheses of high quality freestanding polyselenophene films in boron trifluoride diethyl etherate, J. Electroanal. Chem. 578 (2005) 345–355, https://doi.org/10.1016/j.jelechem.2005.01.016.

[51] Jean Roncali, Conjugated poly(thiophenes): synthesis, functionalization, and applications, Chem. Rev. 92 (4) (1992) 711–738, https://doi.org/10.1021/cr00012a009.

[52] H. Chadli, A. Rahmani, J.L. Sauvajol, Raman spectra of C60 dimer and C60 polymer confined inside a (10, 10) single-walled carbon nanotube, J. Phys. Condens. Matter. 22 (2010), https://doi.org/10.1088/0953-8984/22/14/145303.

[53] B. Sundqvist, Raman identification of C70 monomers and dimers, Diam. Relat. Mater. 73 (2017) 143–147, https://doi.org/10.1016/j.diamond.2016.09.001.

[54] N. Chanunpanich, A. Ulman, Y.M. Strzhemechny, S.A. Schwarz, J. Dornicik, M. Rafailovich, J. Sokolov, A. Janke, H.G. Braun, T. Kratzmüller, Polythiophene grafted on polyethylene film, Mater. Res. Soc. Symp. - Proc. 600 (2000) 203–208, https://doi.org/10.1557/proc-600-203.

[55] R.J. Thorn, K.D. Carlson, G.W. Crabtree, H.H. Wang, States determined by photoelectron spectroscopy in the perchlorate and perrhenate of TMTSF, J. Phys. C Solid State Phys. 18 (1985) 5501–5510, https://doi.org/10.1088/0022-3719/18/28/019.

[56] B.L. Hurley, R.L. Mccreery, Covalent Bonding of Organic Molecules to Cu and Al Alloy 2024 T3 Surfaces via Diazonium Ion Reduction, J. Electrochem. Soc. 151 (2004) B252–B259, https://doi.org/10.1149/1.1687428.

[57] P. Powroźnik, L. Grządziel, W. Jakubik, M. Krzywiecki, Sarin-simulant detection by phthalocyanine/palladium structures: from modeling to real sensor response, Sensors Actuators B. Chem. 273 (2018) 771–777, https://doi.org/10.1016/j.snb.2018.06.101.

[58] O. Gu-ping, G. Wen-ming, J. Shi-chao, Z. Fu-jia, Surface analysis for LiBq4 growing on ITO and CuPc film using atomic force microscopy (AFM) and X-ray photoelectron spectroscopy (XPS), Appl. Surf. Sci. 252 (2006) 3417–3427, https://doi.org/10.1016/j.apsusc.2005.01.042.

[59] M.S. Jagadeesh, G. Bussetti, A. Calloni, R. Yivlialin, L. Brambilla, A. Accogli, E. Gibertini, D. Alliata, C. Goletti, F. Ciccacci, L. Magagnin, C. Castiglioni, L. Duo, Incipient Anion Intercalation of Highly Oriented Pyrolytic Graphite Close to the Oxygen Evolution Potential : A Combined X - ray Photoemission and Raman Spectroscopy Study, J. Phys. Chem. C. 123 (2019) 1790–1797, https://doi.org/10.1021/acs.jpcc.8b09823.

[60] R.J.J. Jansen, H. van Bekkum, XPS of nitrogen-containing functional groups on activated carbon, Carbon N. Y. 33 (1995) 1021–1027, https://doi.org/10.1016/0008-6223(95)00030-H.

[61] T. Teslaru, I. Topala, M. Dobromir, V. Pohoata, L. Curecheriu, N. Dumitrascu, Polythiophene films obtained by polymerization under atmospheric pressure plasma conditions, Mater. Chem. Phys. 169 (2016) 120–127, https://doi.org/10.1016/j.matchemphys.2015.11.038.
[62] B. Canava, J. Vigneron, A. Etcheberry, J.F. Guillemoles, D. Lincot, High resolution XPS studies of Se chemistry of a Cu (In, Ga) Se 2 surface, Appl. Surf. Sci. 202 (2002) 8–14, https://doi.org/10.1016/S0169-4332(02)00186-1.
[63] I. Ikemoto, K. Kikuchi, K. Yahuski, H. Kuroa, K. Kobayashi, X-Ray Photoelectron Spectroscopy of Tetramethyltetraselenapulvalene (TMTSF) complexes, Solid State Commun. 42 (1982) 257–259, https://doi.org/10.1017/CBO9781107415324.004.
[64] G. Beamson, D. Briggs, XPS of Organic Polymers, John Wiley & Sons, Chichester, 1992.
[65] N. Miyoshi, G. Tomita, Production and Reaction of Singlet Oxygen in Aqueous Micellar Solutions Using Pyrene as Photosensitizer, Zeitschrift Fur Naturforsch. B. 33 (1978) 622–627, https://doi.org/10.1515/znb-1978-0612.
[66] M. Wainwright, K. Meegan, C. Loughran, R.M. Giddens, Phenothiazinium photosensitisers, Part VI: Photobactericidal asymmetric derivatives, Dye. Pigment. 82 (2009) 387–391, https://doi.org/10.1016/j.dyepig.2009.02.011.
[67] J. Cai, J. Huang, H. Yu, L. Ji, Synthesis, Characterization, and Photocatalytic Activity of TiO2 Microspheres Functionalized with Porphyrin, Int. J. Photoenergy. 2012 (2012) 1–10, https://doi.org/10.1155/2012/348292.
[68] M. Narutaki, K. Takimiya, T. Otsubo, Y. Harima, H. Zhang, Y. Arki, O. Ito, Synthesis and Photophysical Properties of Two Dual Oligothiophene-Fullerene Linkage Molecules as Photoinduced Long-Distance Charge Separation Systems, J. Org. Chem. 71 (2006) 1761–1768, https://doi.org/10.1021/jo051821v.
[69] T. Yamashiro, Y. Aso, T. Otsubo, H. Tang, Y. Harima, K. Yamashita, Intramolecular Energy Transfer of [60]Fullerene-linked Oligothiophenes, Chem. Lett. 28 (1999) 443–444, https://doi.org/10.1246/cl.1999.443.
[70] K. Matsumoto, M. Fujitsuka, T. Sato, S. Onodera, O. Ito, Photoinduced Electron Transfer from Oligothiophenes / Polythiophene to Fullerenes (C60 / C70) in Solution : Comprehensive Study by Nanosecond Laser Flash Photolysis Method, J. Phys. Chem. B. 104 (2000) 11632–11638, https://doi.org/10.1021/jp002228e.
[71] B. Vileno, M. Lekka, A. Sinekiewicz, P. Marcoux, A.J. Kulik, S. Kasas, S. Catsicas, G. Alfred, L. Forro, Singlet oxygen (1Δg) -mediated oxidation of cellular and subcellular components : ESR and AFM assays, J. Phys. Condens. Mater. 17 (2005) S1471–S1482, https://doi.org/10.1088/0953-8984/17/18/005.